Resonant Driving induced Ferromagnetism in the Fermi Hubbard Model

Ning Sun,[1] Pengfei Zhang,[1] and Hui Zhai[1]

[1]*Institute for Advanced Study, Tsinghua University, Beijing, 100084, China*

(Dated: February 23, 2019)

In this letter we study quantum phases and the phase diagram of a Fermi Hubbard model under periodic driving that has been realized in recent cold atom experiments, in particular, when the driving frequency is nearly resonant with the interaction energy. Due to the driving, the effective Hamiltonian contains a correlated hopping term where the density occupation strongly modifies the hopping strength. Focusing on half filling, in addition to the charge and spin density wave phases, large regions of ferromagnetic phase and phase separation are discovered in the weakly interacting regime. The mechanism of this ferromagnetism is attributed to the correlated hopping because the hopping strength within a ferromagnetic domain is normalized to a larger value than the hopping strength across the domain. Thus, the kinetic energy drives the system into a ferromagnetic phase. We note that this is a different mechanism in contrast to the well-known Stoner mechanism for ferromagnetism where the ferromagnetism is driven by interaction energy.

Recently, tremendous experimental progresses have been made on quantum simulation of the Fermi Hubbard model [1–17]. The progresses include the observation of equilibrium properties such as short-range antiferromagnetic correlations [7–9], hidden antiferromagnetic correlations [10], incommensurate spin correlations [11], canted antiferromagnetic correlations [12] and pairing correlations [13]. In particular, the antiferromagnetic quasi-long-range order has been successfully observed through entropy engineering [14]. The progresses also include non-equilibrium behaviors such as the measurement of optical conductivity [15], and the spin and charge transport coefficients [16, 17].

Studying Fermi Hubbard model with cold atoms also allows us to open up new avenue beyond the traditional condensed matter paradigm. One example is the periodically driven Fermi Hubbard model [18, 19]. Since the typical parameters of a Hubbard model is the hopping strength J and the on-site interaction U, both of which are of the order of electron volt in strongly correlated solid-state materials, it is therefore hard to drive a solid-state material with frequency resonant with any of these two energy scales. However, in cold-atom realization of the Fermi Hubbard model, the typical energy scales for these two parameters are both of the order of hundreds to thousand Hertz, and it is quite easy to drive the optical lattices with such a frequency. When the driving frequency is nearly resonant with the interaction parameter U, the driving can strongly modify the Fermi Hubbard model, as observed in a recent experiments [20, 21]. Hence, it is very promising to study novel physics induced by periodic driving that cannot be accessed in a static system. The goal of this letter is therefore to predict the quantum phases and phase diagram of the nearly resonant driven Fermi Hubbard model that is newly realized in cold atom experiments.

Model. We consider a two-dimensional square lattice periodically modulated along the $\hat{x}$ and $\hat{y}$ directions with a frequency ω and an amplitude A, whose single particle Hamiltonian can be written as

$$\hat{H}_0(t) = \frac{\mathbf{p}^2}{2m} + \hat{V}(x + A\cos(\omega t), y + A\cos(\omega t)) \tag{1}$$

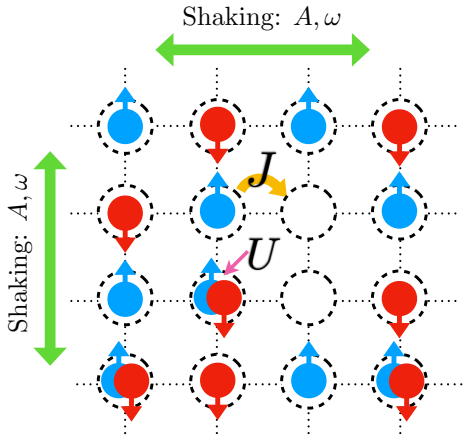

FIG. 1: A schematic of the Fermi Hubbard model on a two-dimensional square lattice. Arrows indicate the direction of shaking. Balls with different colors and arrows indicate fermions with different spins.

where m is the mass of an atom. We can now preform a unitary transformation [22]

$$\hat{U}(t) = \exp(i\mathbf{p}\cdot\mathbf{r}_0(t)/\hbar), \tag{2}$$

where $\mathbf{r}_0(t) = -A\cos(\omega t)(1,1)$ are two-dimensional vectors. This unitary transformation transfers position $\mathbf{r}_0(t)$ into the comoving frame with an extra time-dependent gauge field introduced. The resulting Hamiltonian is written as

$$\hat{H}_0(t) = \frac{(\mathbf{p} - \mathbf{A}(\mathbf{t}))^2}{2m} + \hat{V}(\mathbf{r}), \tag{3}$$

with $\mathbf{A}(t) = m\mathbf{r}_0'(t)$. The Hamiltonian Eq. 3 is equivalent to Eq. 1 but more convenient for the later purpose.

Utilizing the Peierls substitution, the single-band Hamiltonian in a second quantized form can be written as

$$\hat{H}(t) = -J\sum_{\substack{\langle i,j\rangle \\ \sigma=\uparrow,\downarrow}} e^{i\mathbf{d}_{ij}\cdot\mathbf{A}(t)/\hbar}\hat{c}^\dagger_{i\sigma}\hat{c}_{j\sigma} + U\sum_i\left(\hat{n}_{i\uparrow} - \frac{1}{2}\right)\left(\hat{n}_{i\downarrow} - \frac{1}{2}\right), \tag{4}$$

where $\hat{c}_{i\sigma}$ ($\hat{c}^\dagger_{i\sigma}$) is the fermionic annihilation (creation) operator on site i with spin σ, $\hat{n}_{i\sigma}$ is the density operator on site i with spin σ, $\langle \ldots \rangle$ denotes the nearest neighboring sites, and $\mathbf{d_{ij}} = \mathbf{d_i} - \mathbf{d_j}$ with $\mathbf{d_i}$ being the position of the ith lattice site. Throughout this work we focus on the half-filling case and the chemical potential is set to zero.

When the modulation frequency ω is the largest energy scale of the problem, that is to say, it is much larger than both the interaction parameter U and the hopping J, one can do a high-frequency expansion and truncate to the lowest order to obtain an effective time-independent Hamiltonian [23, 24]. The effective Hamiltonian takes the same form as a normal Hubbard model with the only modification that the tunneling coefficient being renormalized by the oscillating gauge field as $\tilde{J} = J\mathcal{B}_0(\mathcal{A})$, where we use $\mathcal{B}_l$ to denote the lth Bessel function and $\mathcal{A} = mA\omega d/\hbar$ the normalized shaking amplitude. d is the distance of two Wannier wave packets in the nearest neighboring lattice sites.

However, this expansion fails when the modulation frequency ω, or lth multiple of it, is comparable to one of the energy scale of the problem, say, the interaction strength U, for which case we call it the lth resonance. In this case, since U is no longer very small comparing with ω while $U - l\hbar\omega$ is a much smaller energy scale, we apply another unitary transformation

$$\hat{R}(t) = \exp(i \sum_j l\omega t \hat{n}_{j\uparrow}\hat{n}_{j\downarrow}), \tag{5}$$

that alters the interaction strength to an effective one $\tilde{U} = U - l\hbar\omega$. Now that $\tilde{U} \sim J \ll U \sim l\hbar\omega$. Moreover, since $\hat{R}(t)$ does not commute with the Hamiltonian, it introduces an additional density dependence to the hopping term, and effectively it alters the gauge field into a spin and density dependent one as follows.

$$\tilde{\mathbf{A}}_{ij,\sigma}(t) = \mathbf{A}(t) - \frac{l\omega t}{d^2}\mathbf{d_{ij}}((1-\hat{n}_{i\bar{\sigma}})\hat{n}_{j\bar{\sigma}} - (1-\hat{n}_{j\bar{\sigma}})\hat{n}_{i\bar{\sigma}})). \tag{6}$$

Now the high frequency expansion can be safely done, and to the lowest order it again results in a time-independent effective Hamiltonian written as

$$\hat{H}_{\text{eff}} = \sum_{\langle i,j\rangle,\sigma} -\hat{J}^{\langle ij\rangle}_{\text{eff},\sigma}\hat{c}^\dagger_{i\sigma}\hat{c}_{j\sigma} + \tilde{U}\sum_i \left(\hat{n}_{i\uparrow} - \frac{1}{2}\right)\left(\hat{n}_{i\downarrow} - \frac{1}{2}\right). \tag{7}$$

Here $\hat{J}^{\langle ij\rangle}_{\text{eff},\sigma}$ is introduced as

$$\hat{J}^{\langle ij\rangle}_{\text{eff},\sigma} = J_0\hat{a}_{ij\bar{\sigma}} + J_1\hat{b}_{ij\bar{\sigma}}, \tag{8}$$

where $\bar{\sigma}$ denotes the complement of σ, $J_0 = J\mathcal{B}_0(\mathcal{A})$, $J_1 = J\mathcal{B}_l(\eta_{ij}\mathcal{A})$ ($\eta_{ij} = \pm 1$ for $(i_x, i_y) = (j_x \pm 1, j_y)$ or $(i_x, i_y = j_x, j_y \pm 1)$), and

$$\hat{a}_{ij\sigma} = (1-\hat{n}_{i\sigma})(1-\hat{n}_{j\sigma}) + \hat{n}_{i\sigma}\hat{n}_{j\sigma}, \tag{9}$$

$$\hat{b}_{ij\sigma} = (-1)^l(1-\hat{n}_{i\sigma})\hat{n}_{j\sigma} + \hat{n}_{i\sigma}(1-\hat{n}_{j\sigma}). \tag{10}$$

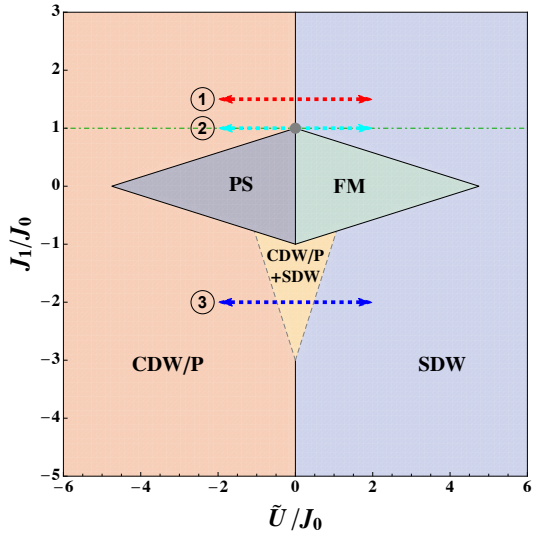

FIG. 2: Phase diagram for the effective Hamiltonian Eq. 7 of a nearly resonantly driven Fermi Hubbard model with even l at half filling. The phase diagram is controlled by two dimensionless parameters, J_1/J_0 and $\tilde{U}/J_0$. "CDW" and "SDW" denote charge and spin density wave order. "P" denotes fermion pairing order. "FM" denotes ferromagnetism. "PS" denotes phase separation into high and low density regimes. Solid lines are first order phase transition and the dashed lines denote the second order phase transition. Dashed arrows mark the lines along which the order parameters are plotted in FIG. 3.

In above, the site dependence of J_1 is made implicitly. Note, however, that for even l the Bessel function $\mathcal{B}_l$ is an even function, in which case η_{ij} can be simply dropped and J_1 becomes a constant. In contrast to the off-resonance case, now the hopping strength depends on the site occupation of fermions. As we will show below, this correlated hopping plays a key role in the emergent new mechanism for the ferromagnetism phase.

Symmetry. Before we delve into solving this effective Hamiltonian, let us first comment on the symmetry of this problem. Note that the original Hubbard model possesses a SO(4) symmetry [25], which is composed of a spin SU(2), generated by $\hat{S}_z = (1/2)\sum_i \hat{c}^\dagger_{i\uparrow}\hat{c}_{i\uparrow} - \hat{c}_{i\downarrow}\hat{c}_{i\downarrow}$, $\hat{S}_+ = \sum_i \hat{c}^\dagger_{i\uparrow}\hat{c}_{i\downarrow}$ and $\hat{S}_- = \hat{S}^\dagger_+$, and a charge SU(2), generated by $\hat{L}_z = -(1/2)\sum_i \hat{c}^\dagger_{i\uparrow}\hat{c}_{i\uparrow} + \hat{c}^\dagger_{i\downarrow}\hat{c}_{i\downarrow} + N_s/2$, $\hat{L}_+ = \sum_i (-1)^i \hat{c}_{i\uparrow}\hat{c}_{i\downarrow}$ and $\hat{L}_- = \hat{L}^\dagger_+$. N_s is the total number of sites. The spin SU(2) ensures that the direction of spin-density-wave (SDW) order parameter can be taken along any direction, and the charge SU(2) ensures the degeneracy of a charge-density-wave (CDW) order and the fermion pairing order (P).

Considering the time-dependent Hamiltonian Eq. 4, it is straightforward to show that the spin SU(2) symmetry stays, yet the charge SU(2) symmetry no longer holds since $\hat{L}_z$ does not commute with the $\sum_{i,\sigma} f_i(t)\hat{n}_{i\sigma}$ term. However, considering the time-independent effective Hamiltonian Eq. 7, one can show that the charge SU(2) symmetry is recovered for even l case though not for odd l case [26]. Hereafter we focus only on the even l case which possesses the same SO(4) symmetry. In addition, it also possesses the particle-hole symmetry

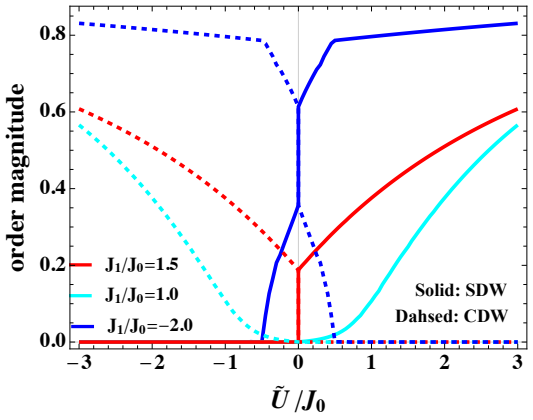

FIG. 3: The CDW order parameter c (dashed lines) and the SDW order parameter s (solid lines) as a function of $\tilde{U}$ for three representative cases labeled as 1-3 in Fig. 2, with $J_1/J_0 = 1.5$, 1.0 and −2.0, respectively.

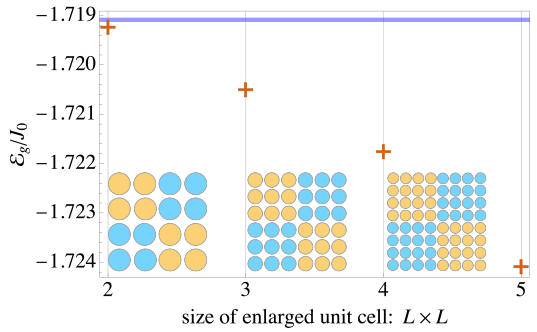

FIG. 4: The mean-field ground state energy (ε_g) as a function of the domain size L for a representative case $J_1 = 0, \tilde{U}/J_0 = -0.2$. The insets show the configuration for 2×2, 3×3 and 4×4 blocks where the CDW and SDW order parameters are uniformly distributed within a domain and take opposite values between neighboring domains. For comparison, the solid line is the mean-field energy when order parameters are all zero.

at half-filling.

Phase Diagram. We present our results on the phase diagram derived from a standard mean-field treatment on this effective Hamiltonian Eq. 7, which is known to be qualitatively reliable for a normal Hubbard model on a square lattice at half-filling (the dot-dashed green line on Fig. 2) because the ordering occurs with infinitesimal weak interaction parameter due to the nesting effect [26, 27]. Thanks to the SO(4) symmetry, we can choose SDW along $\hat{z}$ direction (i.e. $s_i = \langle \hat{n}_{i\uparrow} - \hat{n}_{i\downarrow} \rangle$) and CDW (i.e. $c_i = \langle \hat{n}_{i\uparrow} + \hat{n}_{i\downarrow} \rangle - 1$) as the order parameters in our mean-field theory. Higher order effect will break the degeneracy between CDW and P, but it is beyond the scope of current work.

The phase diagram is shown in Fig. 2, which is controlled by two parameters of J_1/J_0 and $\tilde{U}/J_0$. As a benchmark of our calculation, first of all, note that when $J_1/J_0 = 1$, because of $\hat{a}_{ij\sigma} + \hat{b}_{ij\sigma} = \hat{I}$, the kinetic energy term becomes $-J_0 \sum_{\langle ij \rangle, \sigma} \hat{c}^\dagger_{i\sigma} \hat{c}_{j\sigma}$ and the Hamiltonian recovers the usual Hubbard model. In this case (labeled by 2 and the underlying dot-dashed green line in Fig. 2), the result for the normal Hubbard model is retrieved where we obtain a CDW order of (π, π) with attractive interaction ($\tilde{U} < 0$) and a SDW order of (π, π) with repulsive interaction ($\tilde{U} > 0$). Explicitly, the order parameters are chosen as $s_i = (-1)^{i_x + i_y} s$ and $c_i = (-1)^{i_x + i_y} c$, and $s(c)$ gradually vanishes as $\tilde{U}$ approaches zero from the positive (negative) side. As a result, a second order phase transition occurs at $\tilde{U} = 0$ (gray dot in FIG. 2). This can be seen from the order parameters plotted as a function of $\tilde{U}$, shown as cyan curves in Fig. 3.

Since both CDW and SDW are ordered phases, it should be either a first order transition or a phase co-existence regime in between for more generic situations. As marked by the solid vertical lines in Fig. 2, it is a first order transition on the phase boundary at large $|J_1/J_0|$. The magnitude of order parameters are shown with red lines in Fig. 3 (labeled by 1 in Fig. 2) jump from a finite value to zero at $\tilde{U} \to 0$. In between, a CDW and SDW co-existence regime shows up at certain range of J_1/J_0, as displayed by the yellow region in Fig. 2, whose order parameters are shown with blue lines in Fig. 3 for a representative case (labeled by 3 in Fig. 2).

The most notable feature in Fig. 2 is the middle green and dark gray region. In this region a mean-field ansatz of CDW or SDW orders with ordering vector at (π, π) may not yield any ordered solution. However, when we consider the case of enlarged 2×2, 3×3, up to $L \times L$ domains, and within each domain the CDW and SDW order parameters are uniformly chosen as c and s while in its neighboring domain they are taken as $-c$ and $-s$, the mean-field ansatz does yield ordered solutions. It can be seen from Fig. 4 that the mean-field ground state energy decreases monotonically as L increases. It indicates that the ground state will form large domains with opposite order parameter values. Moreover, minimizing ground state energy yields $c = 0$ and $s \neq 0$ at positive $\tilde{U}$ and $c \neq 0$ and $s = 0$ at negative $\tilde{U}$. Hence, the system with positive $\tilde{U}$ possesses spin order, and the increasing of the domain size means the decreasing of the spin ordering wave vector. Eventually, the wave vector decreases toward zero, and the ground state becomes a ferromagnetic state. In another word, as the domain size becomes larger and larger, the system is essentially made of ferromagnetic domains. For negative $\tilde{U}$ the system tends to be phase separation with high density in one domain and low density in its neighboring domains.

It should be emphasized that both the ferromagnetism and the phase separation regime can occur at small $\tilde{U}$. In fact, it is purely due to the correlated hopping effect in the effective Hamiltonian Eq. 7, which originates essentially from the nearly resonant driving. Considering the mean-field configurations as shown in the insets of Fig. 4, let us look at the mean-field value of the effective hopping strength $\langle \hat{J}^{\langle ij \rangle}_{\text{eff},\sigma} \rangle$ which quantifies how the particle occupation affects the hopping strength. We define $J^{\text{intra}}_{\text{eff},\sigma}$ as $\langle \hat{J}^{\langle ij \rangle}_{\text{eff},\sigma} \rangle$ with i and j in the same domain, and $J^{\text{inter}}_{\text{eff},\sigma}$ as $\langle \hat{J}^{\langle ij \rangle}_{\text{eff},\sigma} \rangle$ with i and j across two

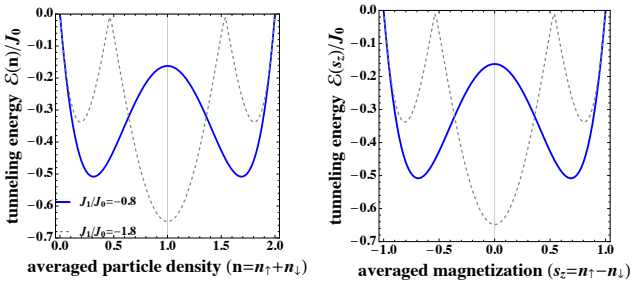

FIG. 5: The mean-field energy with $\tilde{U} = 0$ (a) as a function of total density n with $s_z = 0$ fixed, and (b) as a function of s_z with $n = 1$ fixed. Solid line is for $J_1/J_0 = -0.8$ and the dashed line is for $J_1/J_0 = -1.8$.

neighboring domains. It is straightforward to write down $J^{\rm intra}_{{\rm eff},\sigma}$ and $J^{\rm inter}_{{\rm eff},\sigma}$, respectively, as

$$J^{\rm intra}_{{\rm eff},\sigma} = \frac{1}{2}\left(J_0[1+(c\mp s)^2] + J_1[1-(c\mp s)^2]\right), \qquad (11)$$

$$J^{\rm inter}_{{\rm eff},\sigma} = \frac{1}{2}\left(J_0[1-(c\mp s)^2] + J_1[1+(c\mp s)^2]\right), \qquad (12)$$

where $\mp$ corresponds to different spin components. One can show that when $|J_1| < |J_0|$, $|J^{\rm inter}_{{\rm eff},\sigma}|$ is always smaller than $|J^{\rm intra}_{{\rm eff},\sigma}|$. Hence, the size of the domain tends to increase such that there are more intra-domain links than inter-domain links, and therefore the effective bandwidth becomes larger. For a given filling, a larger bandwidth leads to more kinetic energy gain. $|J_1| < |J_0|$ is precisely the regime where we find ferromagnetism or phase separation in the phase diagram of Fig. 3 with arbitary weak interaction. This regime can be easily accessed when $\mathcal{A}$ is small by exploring a small shaking amplitude.

An alternative way to understand the emergence of this ferromagnetism is to consider a uniform system with $\tilde{U} = 0$. Substitute $\hat{J}^{\langle ij\rangle}_{{\rm eff},\sigma}$ by its mean-field value, it is straightforward to compute the kinetic energy of this uniform system that depends on $n_{i\uparrow}$ and $n_{i\downarrow}$, where $n_\uparrow = (n+s_z)/2$ and $n_\downarrow = (n-s_z)/2$. We plot the kinetic energy as a function of n with $s_z = 0$ in Fig. 5(a) and as a function of s_z with $n = 1$ in Fig. 5(b) for two representative cases of $J_1/J_0 = -0.8$ and -1.8. One can see from Fig. 5(a) that for $J_1/J_0 = -0.8$, there are two local minima with one at $n > 1$ and the other at $n < 1$, who are located symmetrically on two sides of $n = 1$; while for $J_1/J_0 = -1.8$ there is only one minimum located at $n = 1$. Similarly, in Fig. 5(b) for $J_1/J_0 = -0.8$, there are two local minima with one at positive s_z and the other at negative s_z, symmetrically distributed around $s_z = 0$, and for $J_1/J_0 = -1.8$ there is only one minimum at $s_z = 0$. Thus, when the system is constrained with the average $n = 1$ and $s_z = 0$, for the case with $J_1/J_0 = -0.8$, it will actually phase separate into domains with either different n or different s_z, corresponding to either phase separation or ferromagnetism, respectively. The choice is made by the sign of $\tilde{U}$ when a small but finite $\tilde{U}$ perturbation is turned on.

Conclusion and Discussion. In contrast to the well-known Stoner mechanism for ferromagnetism driven by the interaction energy, the most significant finding of this work is to provide an alternative mechanism for the onset of ferromagnetism, which roots in the cooperation between the spin order and the correlated hopping. This is also different from the ferromagnetism due to the super-exchange processes discussed in the experiment of Ref. [20] which requires $\tilde{U}$ to be negative.

We also note that in previous literatures, there are a number of works which have studied the same or similar density-assisted hopping model in one dimension [29–37]. However, none of these papers discovers the ferromagnetic state predicted here. In [29], their method only works for sufficiently large $\tilde{U}$. In [30–32], the authors find that the ground state at half filling can be explained by phase separation for charge but the ferromagnetism is not discussed. In [33], the quantum Monte Carlo they used does not converge for small J_1. The works using bosonization method assume a uniform background, for which they overlook the possibility of ferromagnetism [34–36]. An exact diagonalization calculation with small number of sites also may not be able to capture such physics [37] .

Finally we shall comment on the experimental observation of this ferromagnetism. First of all, the ETH group has realized a resonantly shaking honeycomb lattices with cold Fermi gases where the heating takes over only after relatively long time scale [20, 28]. Secondly, it requires a moderate interaction parameter U, because, on one hand, U is comparable with $\hbar\omega$, and has to be much larger than the bandwidth $\sim J$, and on the other hand, U has to be smaller than the band gap in order to allow the single-band model to be valid, i.e. $\hbar\omega \sim U < \frac{\hbar^2}{md^2}$. This leads to $\mathcal{A} = m\omega Ad/\hbar < A/d$. For small shaking amplitude $A/d < 1$, we then have small $\mathcal{A}$ where $J_0 > J_1 > 0$. In such a parameter regime, we should be able to observe the ferromagnetism. Thirdly, because this ferromagnetism is driven by the kinetic energy, one expects that this ferromagnetism can be observed when temperature is of the order of the bandwidth, which can be accessed now by cold atom experiments where $T/T_F \sim 0.1$ [20]. Finally, the quantum gas microscope techniques can be used to detect real space ferromagnetic domains. Hence, it is quite promising to verify the theoretic expectations experimentally in very near future.

Acknowledgment. This work is supported MOST under Grant No. 2016YFA0301600 and NSFC Grant No. 11734010.

[1] E. Haller, J. Hudson, A. Kelly, D. A. Cotta, B. Peaudecerf, G. D. Bruce and S. Kuhr, *Single-atom imaging of fermions in a quantum-gas microscope*, Nature Physics **11**, 738 (2015).

[2] L. W. Cheuk, M. A. Nichols, M. Okan, T. Gersdorf, V. V. Ramasesh, W. S. Bakr, T. Lompe, and M. W. Zwierlein, *Quantum-Gas Microscope for Fermionic Atoms*, Phys. Rev. Lett. **114**, 193001 (2015).

[3] G. J. A. Edge, R. Anderson, D. Jervis, D. C. McKay, R. Day,

S. Trotzky, and J. H. Thywissen, *Imaging and addressing of individual fermionic atoms in an optical lattice*, Phys. Rev. A **92**, 063406 (2015).

[4] A. Omran, M. Boll, T. A. Hilker, K. Kleinlein, G. Salomon, I. Bloch, and C. Gross, *Microscopic Observation of Pauli Blocking in Degenerate Fermionic Lattice Gases*, Phys. Rev. Lett. **115**, 263001 (2015).

[5] D. Greif, M. F. Parsons, A. Mazurenko, C. S. Chiu, S. Blatt, F. Huber, G. Ji and M. Greiner, *Site-resolved imaging of a fermionic Mott insulator*, Science **351**, 953-957 (2016).

[6] L. W. Cheuk, M. A. Nichols, K. R. Lawrence, M. Okan, H. Zhang, and M. W. Zwierlein, *Observation of 2D Fermionic Mott Insulators of 40K with Single-Site Resolution*, Phys. Rev. Lett. **116**, 235301 (2016).

[7] M. F. Parsons, A. Mazurenko, C. S. Chiu, G. Ji, D. Greif and M. Greiner, *Site-resolved measurement of the spin-correlation function in the Fermi-Hubbard model*, Science **353**, 1253-1256 (2016).

[8] M. Boll, T. A. Hilker, G. Salomon, A. Omran, J. Nespolo, L. Pollet, I. Bloch and C. Gross, *Spin- and density-resolved microscopy of antiferromagnetic correlations in Fermi-Hubbard chains*, Science **353**, 1257-1260 (2016).

[9] L. W. Cheuk, M. A. Nichols, K. R. Lawrence, M. Okan, H. Zhang, E. Khatami, N. Trivedi, T. Paiva, M. Rigol and M. W. Zwierlein, *Observation of spatial charge and spin correlations in the 2D Fermi-Hubbard model*, Science **353**, 1260-1264 (2016).

[10] T. A. Hilker, G. Salomon, F. Grusdt, A. Omran, M. Boll, E. Demler, I. Bloch, C. Gross, *Revealing hidden antiferromagnetic correlations in doped Hubbard chains via string correlators*, Science **357**, 484-487 (2017).

[11] G. Salomon, J. Koepsell, J. Vijayan, T. A. Hilker, J. Nespolo, L. Pollet, I. Bloch, C. Gross, *Direct observation of incommensurate magnetism in Hubbard chains*, arXiv: 1803.08892.

[12] P. T. Brown, D. Mitra, E. Guardado-Sanchez, P. Schaub, S. S. Kondov, E. Khatami, T. Paiva, N. Trivedi, D. A. Huse and W. S. Bakr, *Spin-imbalance in a 2D Fermi-Hubbard system*, Science **357**, 1385-1388 (2017).

[13] D. Mitra, P. T. Brown, E. Guardado-Sanchez, S. S. Kondov, T. Devakul, D. A. Huse, P. Schaub and W. S. Bakr, *Quantum gas microscopy of an attractive Fermi-Hubbard system*, Nature Physics **14**, 173 (2018).

[14] A. Mazurenko, C. S. Chiu, G. Ji, M. F. Parsons, M. Kanasz-Nagy, R. Schmidt, F. Grusdt, E. Demler, D. Greif and M. Greiner, *A cold-atom Fermi-Hubbard antiferromagnet*, Nature **545**, 462-466 (2017).

[15] R. Anderson, F. Wang, P. Xu, V. Venu, S. Trotzky, F. Chevy, and J. H. Thywissen, *Optical conductivity of a quantum gas*, arXiv:1712.09965.

[16] M. A. Nichols, L. W. Cheuk, M. Okan, T. R. Hartke, E. Mendez, T. Senthil, E. Khatami, H. Zhang, and M. W. Zwierlein, *Spin Transport in a Mott Insulator of Ultracold Fermions*, arXiv:1802.10018.

[17] P. T. Brown, D. Mitra, E. Guardado-Sanchez, R. Nourafkan, A. Reymbaut, S. Bergeron, A.-M. S. Tremblay, J. Kokalj, D. A. Huse, P. Schaub, and W. S. Bakr, *Bad metallic transport in a cold atom Fermi-Hubbard system*, arXiv:1802.09456.

[18] M. Bukov, M. Kolodrubetz and A. Polkovnikov, *Schrieffer-Wolff Transformation for Periodically Driven Systems: Strongly Correlated Systems with Artificial Gauge Fields*, Phys. Rev. Lett. **116**, 125301 (2016).

[19] A.P. Itin and M.I. Katsnelson, *Effective Hamiltonians for Rapidly Driven Many-Body Lattice Systems: Induced Exchange Interactions and Density-Dependent Hoppings*, Phys. Rev. Lett. **115**, 075301 (2015).

[20] F. Görg, M. Messer, K. Sandholzer, G. Jotzu, R. Desbuquois and T. Esslinger, *Enhancement and sign change of magnetic correlations in a driven quantum many-body system*, Nature **553**, 481-485 (2018).

[21] W. Xu, W. Morong, H.-Y. Hui, V. W. Scarola, B. DeMarco, *Correlated Spin-Flip Tunneling in a Fermi Lattice Gas*, arXiv:1711.2061.

[22] R. Shankar, Principles of Quantum Mechanics, Springer 1994.

[23] A. Eckardt and E. Anisimovas, *High-frequency approximation for periodically driven quantum systems from a Floquet-space perspective*, New J. Phys **17**, 093039 (2015).

[24] A. Eckardt, *Colloquium: Atomic quantum gases in periodically driven optical lattices*, Rev. Mod. Phys. **89**, 011004 (2017).

[25] C. N. Yang and S. C. Zhang, SO_4 symmetry in a Hubbard model, Mod. Phys. Lett. B **4**, 759 (1990).

[26] Supplementary material for (i) prove the SO(4) symmetry of the effective Hamiltonian for even l, and (ii) describe the mean-field theory.

[27] N. Nagaosa, Quantum Field Theory in Condensed Matter Physics. Springer 1999.

[28] M. Messer, K. Sandholzer, F. Gorg, J. Minguzzi, R. Desbuquois, T. Esslinger, *Floquet dynamics in driven Fermi-Hubbard systems*, arXiv:1808.00506.

[29] R. Strack and D. Vollhardt *Hubbard model with nearest-neighbor and bond-charge interaction: Exact ground-state solution in a wide range of parameters*, Phys. Rev. Lett. **70**, 2637 (1993).

[30] L. Arrachea and A. A. Aligia, *Exact Solution of a Hubbard Chain with Bond-Charge Interaction*, Phys. Rev. Lett.**73**, 2240 (1994).

[31] L. Arrachea, A. A. Aligia and E. Gagliano, *Anomalous Flux Quantization in a Hubbard Ring with Correlated Hopping*, Phys. Rev. Lett.**76**, 4396 (1996).

[32] A. A. Aligia, Liliana Arrachea, and E. R. Gagliano, *Phase diagram of an extended Hubbard model with correlated hopping at half fillings*, Phys. Rev. B **51**, 13774 (1995).

[33] M. Di Liberto, C. E. Creffield, G. I. Japaridze, and C. Morais Smith, *Quantum simulation of correlated-hopping models with fermions in optical lattices*, Phys. Rev. A **89**, 013624 (2014).

[34] G. I. Japaridze and A. P. Kampf, *Weak-coupling phase diagram of the extended Hubbard model with correlated-hopping interaction*, Phys. Rev. B **59**, 12822 (1999).

[35] G. Japaridze and E. Muller-Hartmann, *Electrons with correlated hopping interaction in one dimension*, Ann. Physik 3 (1994) 163-180.

[36] A. A. Aligia and Liliana Arrachea, *Triplet superconductivity in quasi-one-dimensional systems*, Phys. Rev. B **60**, 15332 (1999).

[37] L. Arrachea, A. A. Aligia, E. Gagliano, K. Hallberg, and C. Balseiro, *Superconducting correlations in Hubbard chains with correlated hopping*, Phys. Rev. B **50**, 16044 (1994).